

Metal–Organic Frameworks as Promising Photosensitizers for Photoelectrochemical Water Splitting

Liping Zhang, Ping Cui, Hongbin Yang, Jiazang Chen, Fangxing Xiao, Yuanyuan Guo, Ye Liu, Weina Zhang, Fengwei Huo,* and Bin Liu*

1. Introduction

Since the first discovery of photoelectrochemical (PEC) water splitting by Fujishima and Honda in the 1970s,^[1] artificial photosynthesis that converts solar energy into chemical fuels—mimicking what nature does—has received great attention in the scientific community. Among the various studied materials, titanium dioxide (TiO₂) has attracted the greatest attention due to its nontoxicity, physical and chemical stability, and peculiar electronic and optical properties.^[2] However the wide band gap of TiO₂ limits its absorption of visible light, which restricts the solar energy conversion efficiency. Over the past few years, considerable efforts have been made to tune the photoresponse of TiO₂ to improve the visible light absorption, such as metallic (e.g., Fe, Zr) or non-metallic (e.g., N, F, C, S, B) doping,^[3–9] and dye molecule^[10,11] or narrow band gap semiconductor (e.g., CdS, CdSe) sensitization.^[12–16] Among which, sensitization of TiO₂ appears to be a promising strategy for harvesting solar energy by enhancing visible light absorption and improving charge separation.^[17,18] However, dye sensitizers usually have

low light absorption coefficient and are effective only when they are chemically bound onto the surface of the semiconductor, with performance depending on the surface area as well as structure of the semiconductor.^[19,20] Furthermore, dye molecules are generally catalytically inactive, which have to be combined with molecular catalysts to realize noticeable photocatalytic activities. Alternatively, narrow band gap semiconductors with large light absorption coefficient are frequently used as photosensitizers for TiO₂ in solar energy conversion. However the stability and toxicity for most of the narrow band gap semiconductors remain a serious problem.

In this work, we demonstrate a new type of photosensitizers, for PEC water splitting: metal–organic frameworks (MOFs). MOFs as a new class of hybrid materials possess highly ordered framework structure and large surface area. Due to their fascinating chemical and physical properties, MOFs are expected to be useful in a large scope of applications, including gas storage^[21,22] and separation,^[23] chemical sensing,^[24] biomedicine^[25] and heterogeneous catalysis.^[26,27] More recently, MOFs are emerging as a new type of photocatalyst.^[28] Having combined metal nodes and bridging ligands, MOFs provide the possibilities of periodical arrangement of light harvesting and catalytic components in a single structure, just like the natural photosynthetic system, making them promising candidates for solar energy conversion. Among different types of MOFs, Ti-based MOFs are expected with good photocatalytic properties due to the presence of high density of Ti-oxo clusters.^[29,30] Under light irradiation, electrons are photogenerated in organic ligands and then transferred to Ti-oxo clusters.^[30] Based on a recent study,^[31] MIL-125 (a Ti-based MOF) has a more negative LUMO (lowest unoccupied molecular orbital) level than the conduction band edge of TiO₂, making electron injection from MIL-125 to TiO₂ thermodynamically feasible. Thus herein, we studied a series of Ti-based MOFs as photosensitizers on TiO₂ photoanode for PEC water splitting. Our results showed that the PEC water oxidation performance of TiO₂ could be significantly enhanced by applying MOFs as photosensitizers under visible light illumination.

2. Results and Discussion

Three Ti-based MOFs (MIL-125, MIL-125(NH₂), MIL-125(NH₂)_{1,2}) were studied as photosensitizers for PEC water splitting. The TiO₂/MOF hybrid nanocomposite was prepared on an FTO substrate by a two-step solution phase method. In the first step, vertically oriented, single crystalline TiO₂ nanowire

L. Zhang
Energy Research Institute@NTU
Interdisciplinary Graduate School
Nanyang Technological University
Singapore 637141, Singapore

L. Zhang, Dr. P. Cui, Dr. H. Yang, Dr. J. Chen,
Dr. F. Xiao, Prof. B. Liu
Division of Chemical and Biomolecular Engineering
School of Chemical and Biomedical Engineering
Nanyang Technological University
62 Nanyang Drive, Singapore 637459, Singapore
E-mail: liubin@ntu.edu.sg

L. Zhang, Y. Guo, Y. Liu, Dr. W. Zhang
School of Materials Science and Engineering
Nanyang Technological University
50 Nanyang Avenue, Singapore 639798, Singapore

Prof. F. Huo
Key Laboratory of Flexible Electronics (KLOFE)
and Institute of Advanced Materials (IAM)
Jiangsu National Synergistic Innovation Center
for Advanced Materials (SICAM)
Nanjing Tech University (NanjingTech)
30 South Puzhu Road, Nanjing 211816, P.R. China
E-mail: fengweihuo@outlook.com

This is an open access article under the terms of the Creative Commons Attribution License, which permits use, distribution and reproduction in any medium, provided the original work is properly cited.

DOI: 10.1002/adv.201500243



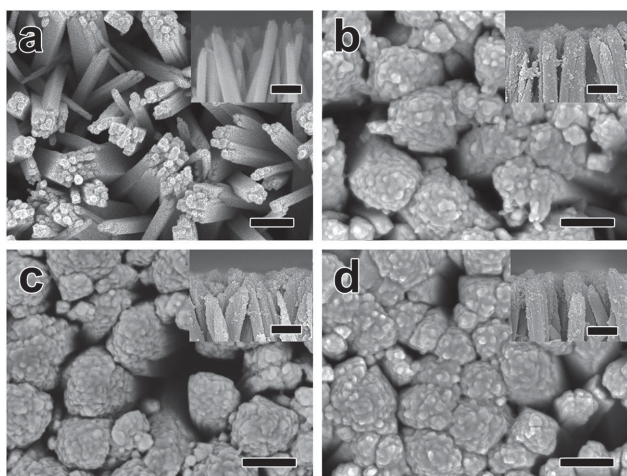


Figure 1. FESEM images of a) TiO₂ nanowire arrays, b) TiO₂/MIL-125 nanowire arrays, c) TiO₂/MIL-125(NH₂) nanowire arrays, and d) TiO₂/MIL-125(NH₂)_{1,2} nanowire arrays. Scale bars: 200 nm.

arrays were grown on FTO substrate based on a hydrothermal method. The as-grown ordered one-dimensional TiO₂ nanostructures possess large surface area as well as short minority carrier diffusion pathways (perpendicular to the nanowire growth direction), which could serve as excellent photoanode for PEC water splitting.^[32,33] Figure 1a and Figure S1 (Supporting Information) show both the top view and cross-sectional view FESEM images of the TiO₂ nanowire arrays, from which the average diameter and length of the TiO₂ nanowires were determined to be around 100 nm and 1.5 μm , respectively.

Subsequently, in the second step, Ti-based MOFs were grown on the surface of TiO₂ nanowires to form a core-shell hybrid nanostructure. In this step, it was found that modification of the TiO₂ surface was critical in promoting the heterogeneous nucleation and growth of MOF nanostructures. Without surface modification, the Ti-based MOF grew homogeneously in solution, resulting in phase segregated TiO₂ and MOF nanostructures (Figure S2, Supporting Information). The ligand (BDC or BDC-NH₂) used to modify TiO₂ has -COOH functional groups, which bind strongly with the surface Ti atom on TiO₂ and thus create nuclei sites for the MOF growth. Figure 1b–d show FESEM images of TiO₂ nanowire arrays coated with MIL-125, MIL-125(NH₂) and MIL-125(NH₂)_{1,2}, respectively. It can be observed that the surface of the nanowires becomes rougher after coating with MOF nanostructures, accompanied by an increase in nanowire diameter, indicating successful coating of MOF on the surface of TiO₂ nanowires. The XRD patterns as displayed in Figure 2a,b also show both diffractions from TiO₂ and MOFs, which match perfectly with the FESEM observation.

Depending on the choices of ligands, the Ti-based MOFs show different light absorption properties. Figure 2c shows the UV–vis diffuse reflectance spectra of TiO₂ and TiO₂/MOF nanocomposites. Both TiO₂ and TiO₂/MIL-125 show similar light absorption onset, which is around 420 nm, suggesting the wide band gap nature for both TiO₂ and MIL-125. Based on the literature,^[34] the HOMO (highest occupied molecular orbital)–LUMO gap of MIL-125 is 3.8 eV; i.e., MIL-125 can only absorb light in the UV spectrum. To reduce the HOMO–LUMO

gap, amine modified ligands were used for growing MIL-125. Amines are strong electron-donating substituents, which could help to raise the HOMO level of MOFs while maintaining the LUMO level, thus reducing the HOMO–LUMO gaps. After amine modification, monoaminated MIL-125(NH₂) shows an obvious red-shift in light absorption towards visible light, while partially diaminated MIL-125(NH₂)_{1,2} possesses an even narrower HOMO–LUMO gap with absorption onset at around 650 nm, which correspond well with the yellow and dark brown colors of MIL-125(NH₂) and MIL-125(NH₂)_{1,2} (Figure S3, Supporting Information). Clearly, ligand modification offers an effective way to tune the HOMO–LUMO gaps of MOFs, thus changing the optical properties.

Photocatalytic properties of as-prepared TiO₂/MOF nanocomposites were evaluated by performing PEC water splitting. Both TiO₂ and TiO₂/MOF samples with fixed sample area were used as the photoanode. Figure 2d displays the J–V curves for water splitting under AM1.5 illumination with UV light cutoff ($\lambda > 420$ nm). It is clear to see that the pristine TiO₂ nanowire electrode has a very small photocurrent density of only 10 $\mu\text{A cm}^{-2}$ at 0.75 V vs. RHE (reversible hydrogen electrode), due to the large band gap of rutile TiO₂ (3.0 eV). When sensitized with Ti-based MOFs, different PEC performances were realized. MIL-125 sensitized TiO₂ showed a comparable PEC performance as the pristine TiO₂ electrode, which is due to the fact that MIL-125 can only absorb UV light. On the contrary, significant improvements in photocurrent were observed in both MIL-125(NH₂) and MIL-125(NH₂)_{1,2} sensitized TiO₂ electrodes, resulting from much enhanced visible light absorption in these aminated MOFs. The LUMO level of MIL-125 is more negative than the conduction band edge of TiO₂,^[31] as a result, electron transfer from MIL-125 to TiO₂ will proceed favorably. As ligand modification merely affects the LUMO level of MOFs,^[34] it is anticipated that the electron transfer from MIL-125(NH₂) or MIL-125(NH₂)_{1,2} to TiO₂ will be unaffected. Upon visible light illumination, electrons in the HOMO level of MIL-125(NH₂) or MIL-125(NH₂)_{1,2} are photoexcited into the LUMO level, which will be quickly injected into the conduction band of TiO₂ and then be transported through TiO₂ to reach the counter electrode to reduce water. Simultaneously, the holes in the HOMO level of MOFs will drive water oxidation to evolve oxygen. Thus, the overall PEC performance will be affected by the light absorption as well as rate of chemical reactions (water reduction and oxidation).

Increasing the MOF layer thickness could increase the photocurrent density because of enhanced light absorption; however, if the MOF layer becomes too thick, the poor electron transport in the MOF layer could lead to significant charge recombination and thus decrease the photocurrent density. To further improve light absorption while at the same time keeping a thin MOF layer to enhance water oxidation kinetics, Au nanoparticles were specifically selected to modify MOF sensitized TiO₂ photoelectrode. Au nanoparticles not only have strong light absorption in the visible solar spectrum due to localized surface plasmon resonance (LSPR), which can be utilized to increase the light absorption cross-section of the photosensitizer, but also have the capability to catalyze water oxidation reaction. MIL-125(NH₂) sensitized TiO₂ was further decorated with Au nanoparticles. Figures S4–S6 (Supporting Information)

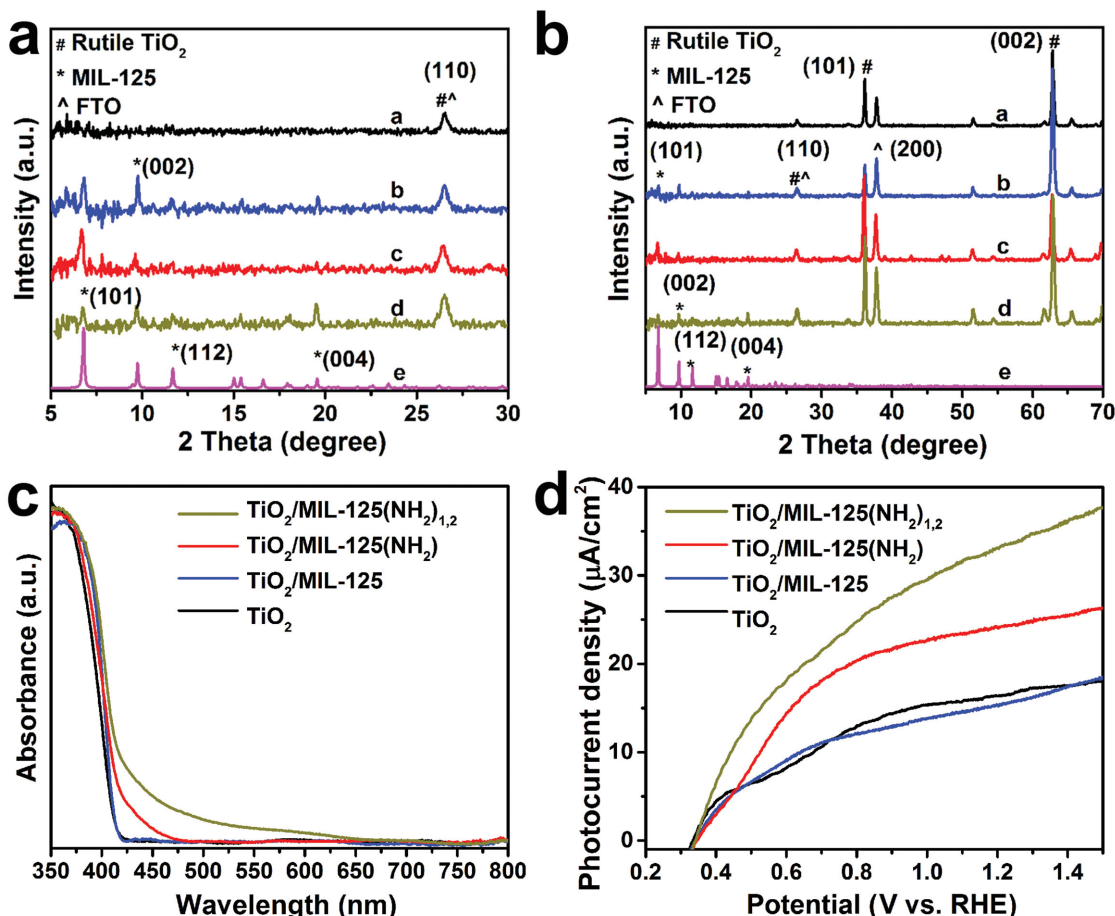


Figure 2. a,b) XRD patterns of TiO₂ and TiO₂/MOF nanocomposites: curve a) TiO₂, b) TiO₂/MIL-125, c) TiO₂/MIL-125(NH₂), d) TiO₂/MIL-125(NH₂)_{1,2} and e) simulated MIL-125). c) UV-vis diffuse reflectance spectra of TiO₂ and TiO₂/MOF nanocomposites. d) J-V curves of TiO₂ and TiO₂/MOF nanocomposites.

show the XRD pattern, XPS spectra and TEM images of Au nanoparticles modified TiO₂/MIL-125(NH₂) nanocomposite. In the wide scan XPS spectra (Figure S5a), the newly appeared N 1s peak in TiO₂/MIL-125(NH₂) and TiO₂/MIL-125(NH₂)/Au suggest the successful coating of MOF on the TiO₂ photoanode. While the Au 4f peaks in TiO₂/MIL-125(NH₂)/Au reveal the successful decoration of Au nanoparticles on MOF coated TiO₂ photoanode. After MOF coating, the O 1s peak at 533 eV can be assigned to the -COO⁻ functional groups from MOF ligand (Figure S5b-d). The chemical states of neither O nor N were changed after Au nanoparticles were further loaded (Figure S5b-f). From TEM images (Figure S6a,b), plenty of Au nanoparticles are clearly observed. The Au nanoparticles are uniformly decorated on the TiO₂/MIL-125(NH₂) nanocomposite as confirmed by the STEM-EDX mapping measurement (Figure S7a-e, Supporting Information). After loading Au NPs, an additional light absorption peak centered at 550 nm resulting from the Au SPR excitation further confirms the successful decoration of Au NPs on TiO₂/MIL-125(NH₂) (Figure S7f).

As electrochemical processes are interfacial, the surface area of the photoelectrode is crucial in our PEC water splitting system. The electrode surface area can be estimated by measuring the double-layer capacitance,^[35] which was done

by cycling the electrode over a narrow potential window (0–0.1 V vs. Ag/AgCl) over which no Faradaic processes took place. The CVs were recorded over a range of scan rates between 1–100 mV sec⁻¹ and the differences between the anodic and cathodic plateau currents were plotted as a function of the scan rate (Figure S8, Supporting Information), which yielded a straight line, intercepting the origin and possessing a slope equal to the double-layer capacitance of the electrode. From Figure S8a, the TiO₂/MIL-125(NH₂) possesses the largest slope—i.e., largest surface area—resulting from the highly porous structure of MOF materials. After incorporating Au nanoparticles, surface area decreased due to blocking of MOF pores by Au nanoparticles.

PEC water oxidation performance was further enhanced by loading Au nanoparticles onto the TiO₂/MIL-125(NH₂) photoelectrode. The stabilized photocurrent was improved by nearly 50% from 20 μA cm⁻² to 30 μA cm⁻² at a bias of 0.75 V vs. RHE under visible light illumination (Figure 3a). As a control experiment, Au nanoparticle modified TiO₂ was also fabricated by the same procedure with TiO₂/MIL-125(NH₂). The enhancement of photocurrent can be attributed to two factors. Firstly, the plasmon-induced visible light absorption of Au NPs can increase the light absorption cross-section of MIL-125(NH₂),

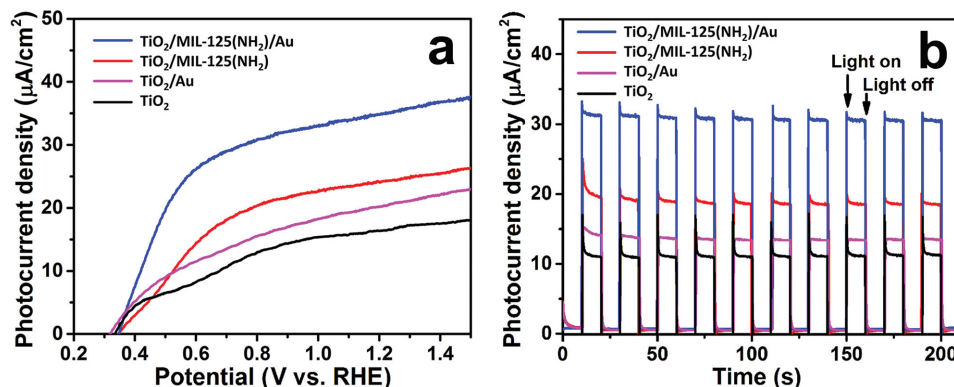


Figure 3. PEC performance of TiO_2 and sensitized TiO_2 nanowire arrays under visible light illumination ($\lambda > 420 \text{ nm}$). a) J - V curves. b) J - t curves upon chopped illumination at 0.75 V vs. RHE.

which in turn increases the light harvesting efficiency. Secondly, upon light illumination, LSPR generates a strong electromagnetic field close to the surface of Au nanoparticles. This electromagnetic field can modify the band structure at the interface between Au and other semiconductor,^[36] which could facilitate charge separation and reduce charge recombination. Besides, the catalytic activity of Au for water oxidation should not be ignored, which also played a role to improve the water oxidation performance.

To get a deeper understanding on the improved PEC water oxidation performance, electrochemical impedance spectroscopy was carried out to study the charge transfer processes across the electrode/electrolyte interface. **Figure 4a** shows the electrochemical impedance Nyquist plots. The semicircles in the Nyquist plot provide information on the charge transfer processes.^[16] From **Figure 4a**, it is clear that $\text{TiO}_2/\text{MIL-125}(\text{NH}_2)$ has a much larger charge transfer resistance at the electrode/electrolyte interface than TiO_2 . This observation should not be surprising as MOFs usually have poor electrocatalytic activities. By decorating Au nanoparticles on $\text{TiO}_2/\text{MIL-125}(\text{NH}_2)$, a reduction in diameter of the semicircle was noticed in the Nyquist plot, indicating improved charge transfer, which could be attributed to the improved charge separation induced by LSPR of Au nanoparticles, as well as enhanced water oxidation kinetics.

The stability of the MOF-sensitized TiO_2 photoelectrodes was examined by recording photocurrent as a function of time during chopped and continuous visible light illumination at a bias of 0.75 V vs. RHE as shown in **Figure 3b** and **Figure S9** (Supporting Information), respectively. All photoelectrodes displayed current spikes, which is due to the slow OER kinetics. However, the current spike became smaller after decorating Au nanoparticles, indicating improved OER kinetics, which is in accordance with our electrochemical impedance data as discussed previously. After reaching steady-state, photocurrent density for TiO_2 , TiO_2/Au , $\text{TiO}_2/\text{MIL-125}(\text{NH}_2)$ and $\text{TiO}_2/\text{MIL-125}(\text{NH}_2)/\text{Au}$ could reach $11 \mu\text{A cm}^{-2}$, $14 \mu\text{A cm}^{-2}$, $20 \mu\text{A cm}^{-2}$, and $32 \mu\text{A cm}^{-2}$, respectively. Furthermore, these photocurrents are highly repeatable during 10 on-off circles, indicating good photostability of the MOF-sensitized electrode under strong oxidizing environment.

An incident photon-to-current conversion efficiency (IPCE) test was further carried out to examine the current contributions. **Figure 3b** shows the IPCE spectra of TiO_2 and MOF-sensitized TiO_2 photoelectrodes, which match well with the results of UV-vis absorption (**Figure S7f**, Supporting Information). In the wavelength region between 420 nm and 500 nm, $\text{TiO}_2/\text{MIL-125}(\text{NH}_2)$ shows an obvious enhancement of IPCE as compared to the pristine TiO_2 , due to improved visible light absorption of $\text{MIL-125}(\text{NH}_2)$, resulting in enhanced overall PEC

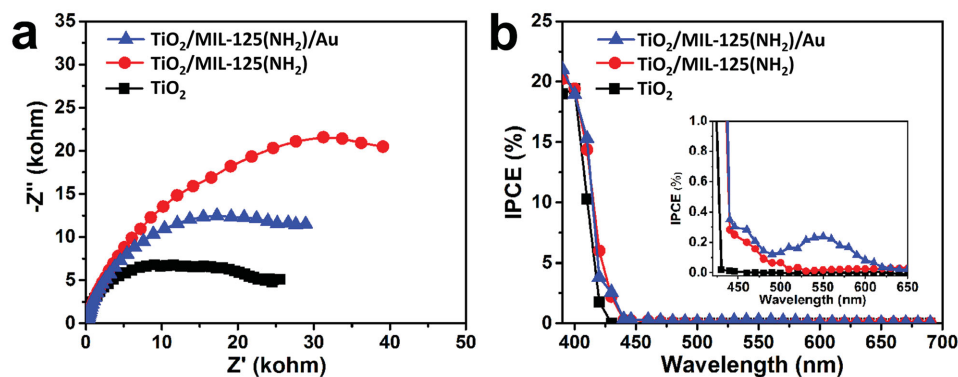


Figure 4. PEC performance of TiO_2 and sensitized TiO_2 nanowire arrays under visible light illumination ($\lambda > 420 \text{ nm}$). a) Nyquist plots. b) IPCE curves.

performance. Loading Au nanoparticles on TiO₂/MIL-125(NH₂) creates an addition IPCE peak centered at 550 nm, arising from the LSPR absorption of Au. It is clear that modification of MIL-125(NH₂) and Au nanoparticles on TiO₂ nanowires significantly improves the visible light absorption and thus enhances the PEC water oxidation performance.

The advantages of using MOFs as photosensitizers are as following: first, the great chemical tailorability enables tuning of the optical and catalytic properties of MOFs at the molecular scale, which can benefit both the light absorption as well as catalytic reactions; second, the highly porous structure of MOFs can also be utilized to incorporate other functional molecules such as photosensitizers or molecular catalysts to work synergistically to improve the photocatalytic efficiency.

3. Conclusions

In summary, Ti-based MOFs have been demonstrated as promising photosensitizers for PEC water splitting. When applied as the photoanode for solar water oxidation, the photocurrent of TiO₂ nanowire photoelectrode could be improved by nearly 100% under visible light through sensitization with aminated Ti-based MOFs. By coupling with plasmonic Au nanoparticles, the light absorption efficiency could be further improved due to the LSPR effect. Considering the diversity of MOFs, a large number of MOFs are expected to work as promising photosensitizers or photocatalysts for solar-driven energy conversion and/or environmental remediation.

4. Experimental Section

Materials: All chemicals were purchased from Sigma-Aldrich without further purification. Fluorine-doped SnO₂ (FTO) glass was purchased from Ltech Scientific Supply.

Growth of TiO₂ Nanowire Arrays on FTO: Oriented rutile TiO₂ nanowire arrays were grown on FTO substrate using a hydrothermal method based on our previous report.^[37] Briefly, 0.83 mL of tetra-n-butyl orthotitanate (TBOT) was mixed with 50 mL of 6 M hydrochloric acid and stirred for 5 min. Afterwards, the growth solution was transferred into a 100 mL Teflon-lined stainless steel autoclave, followed by placing a few pieces of pre-cleaned FTO glass. The hydrothermal reaction was conducted in an electronic oven at 150 °C for 5 h. After reaction, the TiO₂ covered FTO glass was taken out, rinsed thoroughly with deionized water and dried with flowing nitrogen. To improve the crystallinity and conductivity of TiO₂ nanowire arrays, further annealing was performed in air at 450 °C for 30 min.

Preparation of TiO₂/MOF Nanocomposites: TiO₂ nanowires were firstly modified with 1,4-benzenedicarboxylate(BDC) or BDC-NH₂, which are the ligands used for growing MIL-125 and MIL-125-NH₂ respectively. In a particular experiment, 4 pieces of FTO covered by TiO₂ nanowire arrays were immersed in 4 mL of 20 mM BDC (DMF) or BDC-NH₂ (DMF) solution, and kept at 120 °C for 3 h. To grow TiO₂/MOFs composites, redistilled dimethylformamide (DMF) and methanol (MeOH) were used as the solvent. To 5 mL of DMF/MeOH (v/v = 9/1), 0.3 mmol of BDC and 26 μL of TBOT were firstly mixed in a 20 mL Teflon-lined autoclave, to which four pieces of FTO covered with TiO₂ nanowires were placed against the wall of Teflon-liner with the TiO₂ side facing down. The solvothermal reaction was conducted at 150 °C for 72 h to grow TiO₂/MIL-125. TiO₂/MIL-125(NH₂) and TiO₂/MIL-125(NH₂)_{1,2} were prepared using the same protocol with the

same amount of BDC-NH₂ ligand and BDC-(NH₂)₂/BDC-(NH₂) ligand (molar ratio, 1/9), respectively.

Preparation of TiO₂/MIL-125(NH₂)/Au Nanocomposite: HAuCl₄ was used as gold precursor to prepare Au nanoparticles. Firstly, 2 mM HAuCl₄ (MeOH) solution was prepared and the pH was adjusted to 7. Subsequently, TiO₂/MIL-125(NH₂) samples preheated at 120 °C for 10 h were soaked into the HAuCl₄ solution for 3 h, followed by washing with MeOH. After drying, gold precursors were reduced by 0.2 M NaBH₄ solution for 5 min.

Characterization: X-ray diffraction (XRD) patterns were collected on a Bruker AXS D8 Advance diffractometer using nickel-filtered Cu K α radiation ($\lambda = 1.5406 \text{ \AA}$). Field emission scanning electron microscope (FESEM) images were taken on a JEOL JSM-7600 with an accelerating voltage of 5 kV. Transmission electron microscopy (TEM) images were taken on a JEOL JEM 2101F at an accelerating voltage of 200 kV. STEM-EDX elemental mapping was conducted on a JEOL JEM 2100F. UV-visible spectra were recorded using a Perkin-Elmer Lambda 900 UV-vis-NIR spectrometer equipped with an integrating sphere. X-ray photoelectron spectroscopy (XPS) measurements were conducted on an ESCALAB 250 photoelectron spectrometer (Thermo Fisher Scientific) at 2.4×10^{-10} mbar using a monochromatic Al K α X-ray beam (1486.60 eV). Binding energies (BE) were calibrated to the carbon BE of 284.60 eV.

Photoelectrochemical Measurements: Photoelectrochemical properties of TiO₂/MOF nanocomposites were studied on CHI 660D electrochemical workstation in a standard three-electrode setup with Ag/AgCl (3M NaCl) as the reference electrode and a platinum plate as the counter electrode under simulated sunlight from a 300-Watt Xenon lamp (Newport, Oriel, 91160) equipped with an AM 1.5G filter (Newport, 81094) and a 420 nm long pass filter (Newport, FSQ-GG420). The light source was calibrated using a standard Si photodiode. In all cases, a 0.5 M Na₂SO₄ solution (pH = 6.5) was used as the electrolyte. All potentials were converted to values relative to RHE using the following equation:

$$E_{\text{RHE}} = E_{\text{Ag/AgCl}} + 0.0591 \times \text{pH} + E_{\text{Ag/AgCl}}^{\circ} \quad (1)$$

where $E_{\text{Ag/AgCl}}^{\circ}$ is the standard potential of Ag/AgCl relative to RHE at 25 °C (0.197 V). The working area of the photoelectrode was fixed at 0.25 cm² for each experiment. The electrochemical impedance spectroscopy measurements were performed by applying a frequency ranging from 10⁻² to 10⁵ Hz with AC amplitude of 10 mV under visible light illumination (420 nm cut-off) at open-circuit voltage condition. The incident photon-to-current conversion efficiency (IPCE) was measured at a bias of 0.2 V vs. Ag/AgCl. The monochromatic light was supplied by a 300-Watt Xe lamp irradiation through a monochromator (Newport). A chopper was placed in front of the monochromator, and the signal was collected using a lock-in radiometry (Merlin) after amplification by the current preamplifier.

Supporting Information

Supporting Information is available from the Wiley Online Library or from the author.

Acknowledgements

This work was supported by the Nanyang Technological University Startup grant: M4080977.120, the Singapore Ministry of Education Academic Research Fund (AcRF) Tier 1: M4011021.120, the Singapore Ministry of Education Academic Research Fund (AcRF) Tier 2: M4020230.070, Singapore A*Star Public Sector Funding (PSF): M4070232.120, and Singapore A*Star SERC grant: M4070178.120.

Received: July 8, 2015

Revised: August 21, 2015

Published online: November 19, 2015

- [1] A. Fujishima, K. Honda, *Nature* **1972**, 37.
- [2] Y. Zhang, Z.-R. Tang, X. Fu, Y.-J. Xu, *ACS Nano* **2010**, 4, 7303.
- [3] L. M. Liu, X.-F. Lang, H.-Y. Wang, X. W. Lou, E. S. Aydil, *Energ. Environ. Sci.* **2014**, 7, 2592.
- [4] H. M. Liu, C. Chen, S. C. Liu, Andrews, C. Hahn, P. Yang, *J. Am. Chem. Soc.* **2013**, 135, 9995.
- [5] R. Asahi, T. Morikawa, T. Ohwaki, K. Aoki, Y. Taga, *Science* **2001**, 293, 269.
- [6] J. Resasco, N. P. Dasgupta, J. R. Rosell, J. Guo, P. Yang, *J. Am. Chem. Soc.* **2014**, 136, 10521.
- [7] S.H. Shen, J. N. Chen, L. Cai, F. Ren, L. J. Guo, *J. Materiomics*. **2015**, 2, 134.
- [8] Z. R. He, J. Z. Xiao, F. Xia, K. Kajiyoshi, C. Samart, H. B. Zhang, *Appl. Surf. Sci.* **2014**, 313, 633.
- [9] M. M. Momeni, Y. Ghayeb, *J. Electroanal. Chem.* **2015**, 751, 43.
- [10] U. Bach, D. Lupo, P. Comte, J. Moser, F. Weissörtel, J. Salbeck, H. Spreitzer, M. Grätzel, *Nature* **1998**, 395, 583.
- [11] J. R. Swierk, D. D. Méndez-Hernández, N. S. McCool, P. Liddell, Y. Terazono, I. Pahk, J. J. Tomlin, N. V. Oster, T. A. Moore, A. L. Moore, *Proc. Natl. Acad. Sci. USA* **2015**, 112, 1681.
- [12] H. Wang, L. Zhang, Z. Chen, J. Hu, S. Li, Z. Wang, J. Liu, X. Wang, *Chem. Soc. Rev* **2014**, 43, 5234.
- [13] Y-M. Zhu, R-L Wang, W-P Zhang, H-Y Ge, L. Li, *Appl. Surf. Sci.* **2014**, 315, 149.
- [14] F.-X. Xiao, J. Miao, B. Liu, *J. Am. Chem. Soc.* **2014**, 136, 1559.
- [15] H. B. Yang, J. Miao, S.-F. Hung, F. Huo, H. M. Chen, B. Liu, *ACS Nano* **2014**, 8, 10403.
- [16] F.-X. Xiao, J. Miao, H.-Y. Wang, H. Yang, J. Chen, B. Liu, *Nanoscale* **2014**, 6, 6727.
- [17] J. Han, Z. Liu, K. Guo, X. Zhang, T. Hong, B. Wang, *Appl. Catal. B-Environ.* **2015**, 179, 61.
- [18] T. Hong, Z. Liu, H. Liu, J. Liu, X. Zhang, J. Han, *J. Mater. Chem. A* **2015**, 3, 4239.
- [19] J. R. Swierk, N. S. McCool, T. P. Saunders, G. D. Barber, T. E. Mallouk, *J. Am. Chem. Soc.* **2014**, 136, 10974.
- [20] X. Feng, K. Zhu, A. J. Frank, C. A. Grimes, T. E. Mallouk, *Angew. Chem.* **2012**, 124, 2781.
- [21] R. B. Getman, Y.-S. Bae, C. E. Wilmer, R. Q. Snurr, *Chem. Rev.* **2011**, 112, 703.
- [22] L. J. Murray, M. Dincă, J. R. Long, *Chem. Soc. Rev.* **2009**, 38, 1294.
- [23] J.-R. Li, J. Sculley, H.-C. Zhou, *Chem. Rev.* **2011**, 112, 869.
- [24] G. Lu, J. T. Hupp, *J. Am. Chem. Soc.* **2010**, 132, 7832.
- [25] P. Horcajada, R. Gref, T. Baati, P. K. Allan, G. Maurin, P. Couvreur, G. Férey, R. E. Morris, C. Serre, *Chem. Rev.* **2011**, 112, 1232.
- [26] W. Zhang, G. Lu, C. Cui, Y. Liu, S. Li, W. Yan, C. Xing, Y. R. Chi, Y. Yang, F. Huo, *Adv. Mater.* **2014**, 26, 4056.
- [27] G. Lu, S. Li, Z. Guo, O. K. Farha, B. G. Hauser, X. Qi, Y. Wang, X. Wang, S. Han, X. Liu, *Nat. Chem.* **2012**, 4, 310.
- [28] J.-L. Wang, C. Wang, W. Lin, *ACS Catal.* **2012**, 2, 2630.
- [29] M. Dan-Hardi, C. Serre, T. Frot, L. Rozes, G. Maurin, C. Sanchez, G. Férey, *J. Am. Chem. Soc.* **2009**, 131, 10857.
- [30] M. De Miguel, F. Ragon, T. Devic, C. Serre, P. Horcajada, H. García, *ChemPhysChem* **2012**, 13, 3651.
- [31] K. T. Butler, C. H. Hendon, A. Walsh, *J. Am. Chem. Soc.* **2014**, 136, 2703.
- [32] I. Hochbaum, P. Yang, *Chem. Rev.* **2009**, 110, 527.
- [33] Y. J. Hwang, C. Hahn, B. Liu, P. Yang, *ACS Nano* **2012**, 6, 5060.
- [34] H. Hendon, D. Tiana, M. Fontecave, C. M. Sanchez, L. D'arras, C. Sassoie, L. Rozes, C. Mellot-Draznieks, A. Walsh, *J. Am. Chem. Soc.* **2013**, 135, 10942.
- [35] Y. Surendranath, D. G. Nocera, *Oxygen Evolution Reaction Chemistry of Oxide-Based Electrodes*, John Wiley & Sons, Cambridge, MA, USA **2012**.
- [36] H. M. Chen, C. K. Chen, C.-J. Chen, L.-C. Cheng, P. C. Wu, B. H. Cheng, Y. Z. Ho, M. L. Tseng, Y.-Y. Hsu, T.-S. Chan, *ACS Nano* **2012**, 6, 7362.
- [37] B. Liu, E. S. Aydil, *J. Am. Chem. Soc.* **2009**, 131, 3985.